Title

Biodistribution of Antibody-MS2 Viral Capsid Conjugates in Breast Cancer Models

Journal

Molecular Pharmaceutics, 13(11)

ISSN

1543-8384

Authors

Aanei, Ioana L
ElSohly, Adel M
Farkas, Michelle E
et al.

Publication Date

2016-11-07

DOI

10.1021/acs.molpharmaceut.6b00566

Peer reviewed

molecular pharmaceutics

Article

pubs.acs.org/molecularpharmaceutics

Biodistribution of Antibody-MS2 Viral Capsid Conjugates in Breast Cancer Models

Ioana L. Aanei,[†,‡] Adel M. ElSohly,[†] Michelle E. Farkas,[†] Chawita Netirojjanakul,[†] Melanie Regan,[§] Stephanie Taylor Murphy,[§] James P. O'Neil,[‡] Youngho Seo,[§] and Matthew B. Francis*[,†,‡]

[†]Department of Chemistry, University of California, Berkeley, Berkeley, California 94720, United States

[‡]Molecular Biophysics and Integrated Bioimaging Division, Lawrence Berkeley National Laboratories, Berkeley, California 94720, United States

[§]Department of Radiology and Biomedical Imaging, University of California, San Francisco, San Francisco, California 94143, United States

Supporting Information

ABSTRACT: A variety of nanoscale scaffolds, including virus-like particles (VLPs), are being developed for biomedical applications; however, little information is available about their *in vivo* behavior. Targeted nanoparticles are particularly valuable as diagnostic and therapeutic carriers because they can increase the signal-to-background ratio of imaging agents, improve the efficacy of drugs, and reduce adverse effects by concentrating the therapeutic molecule in the region of interest. The genome-free capsid of bacteriophage MS2 has several features that make it well-suited for use in delivery applications, such as facile production and modification, the ability to display multiple copies of targeting ligands, and the capacity to deliver large payloads. Anti-EGFR antibodies were conjugated to MS2 capsids to construct nanoparticles targeted toward receptors overexpressed on breast cancer cells. The MS2 agents showed good stability in physiological conditions up to 2 days and specific binding to the targeted receptors in *in vitro* experiments. Capsids radiolabeled with ^{64}Cu isotopes were injected into mice possessing tumor xenografts, and both positron emission tomography−computed tomography (PET/CT) and scintillation counting of the organs *ex vivo* were used to determine the localization of the agents. The capsids exhibit surprisingly long circulation times (10−15% ID/g in blood at 24 h) and moderate tumor uptake (2−5% ID/g). However, the targeting antibodies did not lead to increased uptake *in vivo* despite *in vitro* enhancements, suggesting that extravasation is a limiting factor for delivery to tumors by these particles.

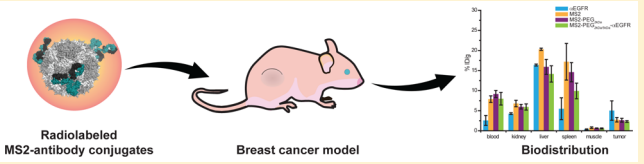

KEYWORDS: *bacteriophage MS2, tumor targeting, antibody targeting, bioconjugation, PET imaging*

INTRODUCTION

Despite numerous advances over the past several decades, the effective detection and treatment of cancer remain challenging.[1] The toxicity of many antitumor drugs makes achieving therapeutic concentrations without severe systemic side effects very difficult.[2] To address these issues, significant efforts have been dedicated to the design of carriers that can deliver the desired cargo selectively to tumor sites. Synthetic platforms, such as polymers,[3] dendrimers,[4,5] liposomes,[6,7] and the protein cage architectures of plant viruses[8,9] and bacteriophages,[10] have been investigated for their potential to serve as *in vivo* delivery vehicles. Most of these vehicles rely on the size of the nanoparticles to take advantage of the increased permeability of the vasculature in the tumor vicinity relative to the rest of the circulatory system to promote passive accumulation.[11] This phenomenon, referred to as the enhanced permeability and retention (EPR) effect,[12−14] is attributed to large spaces between endothelial cells in blood vessels formed during tumor growth[15] and poor drainage by tumor lymphatic systems.[16] Passive targeting of nanoparticles in the 10−100 nm size range has been shown to result in increased tumor accumulation when compared to small molecules.[13] However, there are numerous challenges in generating monodisperse nanoparticles with controlled size in this size range, which is believed to be ideal for tumor uptake via EPR.[13,17] Different types of targeting groups (small molecules,[18,19] aptamers,[20] peptides,[21,22] glycans,[23] antibodies[24−27]) have been used to decorate nanoparticles with the hope of increasing their homing to the tumor. Among these moieties, antibodies have the advantages of widespread availability, as well as high specificity and affinity for their targets. Liposomes that are decorated with antibodies (immunoliposomes) are some of the most advanced nanoparticles on the way to clinical applications and establish the potential of antibodies to be used as targeting moieties on nanoscale carriers *in vivo*.[28,29]

Protein cages have also drawn attention for their ability to carry increased levels of cargo molecules.[29] In addition, protein-

Received: June 22, 2016
Revised: August 21, 2016
Accepted: September 9, 2016
Published: September 9, 2016

DOI: 10.1021/acs.molpharmaceut.6b00566
Mol. Pharmaceutics 2016, 13, 3764−3772

based delivery agents have several advantages over polymer-based platforms, such as homogeneity, biocompatibility, and biodegradability.[30] Although great strides are being made in the tailoring of the *in vivo* properties of protein carriers, most nanoparticles still suffer from rapid clearance from the body due to the reticuloendothelial system (RES) comprising the liver and spleen.[31,32] For example, upon intravenous administration of the Cowpea Mosaic Virus (CPMV) to mouse models,[33,34] the particles localize mainly in the liver and the spleen, are rapidly cleared from plasma, and reach undetectable levels within 20 min. Similarly, the Potato Virus X (PVX) has a short half-life *in vivo* of only 12.5 min.[35] The Cowpea Chlorotic Mottle Virus (CCMV) and Heat Shock Protein (Hsp) also exhibit short circulation times, with less than 1% of the injected dose per gram (% ID/g) still present in the mouse blood at 24 h postinjection.[36]

Recent studies suggest that modification of the surface of nanoparticles with passivating layers, such as polyethylene glycol (PEG), can delay systemic clearance, thus allowing for increased tumor homing.[37] The immunogenicity of viral capsids could also be mitigated by PEGylation of virus-like particle (VLP) constructs, based on studies showing that antibody recognition of the viral capsid proteins can be decreased by PEG chains.[38−41] However, additional research is required to develop a comprehensive understanding of VLP behavior *in vivo*, including biodistribution, clearance rates, immunogenicity, and toxicology, in the interest of facilitating the translation of virus capsid-based nanomedicines from the research laboratory to the clinic.[42]

Herein, we describe a targeted nanoscale imaging platform based on bacteriophage MS2, the VLPs of which self-assemble from 180 copies of a single coat protein (13.8 kDa) into monodisperse, 27 nm icosahedral capsids. MS2 capsids are biodegradable, stable under a variety of temperature, pH, and solvent conditions, and easily synthesized and purified in large quantities.[21] Recently, our group has designed orthogonal chemistries to allow the exterior and interior surfaces to be modified independently.[21,43−46] Through judicious use of these reactions, the viral capsid can house multiple copies of a given drug molecule or imaging agent, potentially offering a significant increase in therapeutic index[20,45,47] or signal intensity,[48,49] respectively. The capsid exterior has also been endowed with cell-specific targeting capabilities via the appendage of receptor-specific antibodies on the external surface. Given the potential of MS2 as a drug delivery and imaging agent, and its success in *in vitro* experiments,[46,50] the *in vivo* behavior of constructs based on this scaffold warrants investigation. The study presented herein therefore lays the foundation for the development of the MS2 bacteriophage into a tailorable delivery system for many future applications.

MATERIALS AND METHODS

Materials. Unless otherwise noted, all chemicals and solvents were of analytical grade and used as received from commercial sources. Anti-EGFR human IgG1 monoclonal antibody was obtained from Eureka Therapeutics, Inc. (Emeryville, CA). All polyethylene glycol (PEG) derivatives were purchased from Laysan Bio, Inc. (Arab, AL). All cell culture reagents, including normal mouse serum, were obtained from Gibco/Thermo Fisher (Waltham, MA) unless otherwise noted. Maleimide-DOTA (1,4,7,10-tetraazacyclododecane-1,4,7-tris-acetic acid-10-maleimidoethylacetamide) and pSCN-Bn-NOTA (2-*S*-(4-isothiocyanatobenzyl)-1,4,7-triazacyclononane-1,4,7-triacetic acid) were purchased from Macrocyclics (Dallas, TX). Maleimide-NOTA (2,2′-(7-(2-((2-(2,5-dioxo-2,5-dihydro-1*H*-pyrrol-1-yl)ethyl)amino)-2-oxoethyl)-1,4,7-triazononane-1,4-diyl)diacetic acid), maleimide-NOTA-GA (2,2′-(7-(1-carboxy-4-((2-(2,5-dioxo-2,5-dihydro-1*H*-pyrrol-1-yl)ethyl)-amino)-4-oxobutyl)-1,4,7-triazonane-1,4-diyl)diacetic acid), and maleimide-DOTA-GA (2,2′,2″-(10-(1-carboxy-4-((2-(2,5-dioxo-2,5-dihydro-1*H*-pyrrol-1-yl)ethyl)amino)-4-oxobutyl)-1,4,7,10-tetraazacyclododecane-1,4,7-triyl)triacetic acid) were purchased from CheMatech (Dijon, France). Ethylenediaminetetraacetic acid (EDTA) disodium salt and potassium phosphate dibasic were purchased from EMD Chemicals Inc. (Darmstadt, Germany). Copper-64 was purchased from the Medical Cyclotron Laboratory, University of Wisconsin. Saline (sodium chloride) solution was Injection USP, 0.9% from APP Pharmaceuticals (Schaumburg, IL).

Methods. *Synthesis and Characterization of MS2−Ab Conjugates.* The protocol for constructing MS2−Ab conjugates was described recently.[46] For full details, please see the Supporting Information.

Immunogenicity Assays. In order to investigate the immune response that the capsids might trigger in a living system, we contracted an outside company, Pacific Bio Laboratories, to test the amount of antibody produced upon tail vein injections of MS2 conjugates. Mice with intact immune systems (female Balb/c, 3 mice per group) were injected intravenously (iv) with 100 μL of agent in sterile saline at $t = 0$ and with a second dose at 3 weeks. Blood samples were obtained before the first injection and at 2, 4, and 8 weeks. The amount of antibody present was determined using commercially available ELISA kits for IgM and IgG quantification. The experimental procedure details are described in the Supporting Information.

Radiolabeling of MS2 Conjugates. To a 100 μM sample of protein (based on capsid monomer) in 10 mM potassium phosphate buffer, pH 7.2, was added 10 equiv of maleimide-chelator from a 10 mM stock in DMSO. The reaction was allowed to proceed for 4 h at room temperature and was purified using a Nap-10 Sephadex size exclusion column (GE Healthcare, Pittsburgh, PA) equilibrated with phosphate buffer, pH 6.5 and 100 kDa molecular weight cutoff (MWCO) spin concentrators (Millipore, Billerica, MA). For the Ab-NOTA samples, the antibodies were first reacted with 200 equiv of pSCN-Bn-NOTA at 37 °C for 24 h. The reaction was stopped by using a Nap-5 desalting column, and the purified antibody was concentrated to 10−20 μM using a 30 kDa spin concentrator (Millipore).

The ^{64}Cu copper stock (20−30 mCi, ∼200 μL) was diluted with 1 mL of 0.1 M ammonium citrate buffer, pH 6.2 to generate a final volume of ∼1200 μL at pH 5.5 (determined by pH paper). Each reaction tube was then charged with 100−400 μL of diluted ^{64}Cu solution and 50−150 μL of the MS2 conjugates (200 μM in capsid monomer). The complexation reactions were allowed to proceed for 2 h at room temperature and then purified using Nap-5 or Nap-10 columns. Samples were subsequently concentrated using 100 kDa MWCO spin concentrators. Centrifugation was performed at 10,000 rpm for 5 min per round of concentrating until the desired volume was reached.

In Vitro Stability Studies. Concentrated ^{64}Cu-chelator-MS2 conjugates (∼300 μCi in 20 μL) were added to PBS or 100% mouse serum to a final volume of 200 μL (1:9 v/v). The samples were then incubated at 37 °C for a predetermined time using a temperature-controlled heat block (VWR, Radnor, PA).

DOI: 10.1021/acs.molpharmaceut.6b00566
Mol. Pharmaceutics 2016, 13, 3764−3772

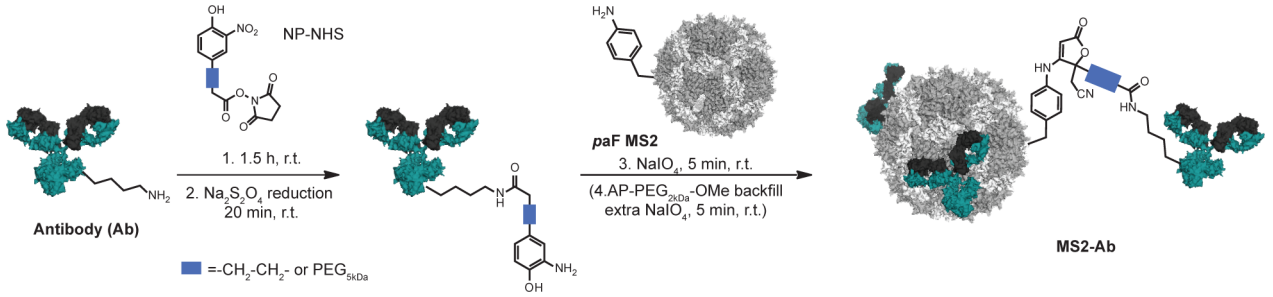

Figure 1. Generation of MS2−antibody conjugates. Nitrophenol (NP) groups were attached to antibodies (Ab) via lysine modification using NP-NHS. The nitrophenol groups were then reduced to yield aminophenol−antibody conjugates (AP−Ab) by addition of $Na_2S_2O_4$. The resulting AP−Ab were coupled to *p*-aminophenylalanine (*p*aF) MS2 via an oxidative coupling using $NaIO_4$ as oxidant.

Aliquots were drawn from the samples at 1, 4, 8, 24, and 48 h time points, and injected onto a PolySep GFC-P5000 (Phenomenex, Torrance, CA) size exclusion chromatography column (300 × 7.8 mm, 5 μm particle size, 500 Å pore size; column flow rate 1.5 mL/min of 10 mM KH_2PO_4 containing 1 mM disodium EDTA, pH 7.2). The HPLC system consisted of a 590 HPLC pump (Waters, Milford, MA), UV detector operating at 280 nm (Linear Systems, Fremont, CA), model 105S-1 high-sensitivity radiation detector with 1 cm^3 CsI (T1) scintillating crystal coupled to a 1 cm^2 Si PIN photodiode/low-noise preamplifier (Carroll-Ramsey Associates, Berkeley, CA), and fluorescence detector (Spectra system FL3000, Thermo Separation Products, St. Peters, MO). Chromatography traces were collected using PeakSimple data system and software (SRI Instruments, Torrance, CA), and analyzed using the Gaussian multipeak fitting feature of the OriginPro software v. 8.6.0 (OriginLab, Northampton, MA).

PET/CT and Biodistribution Studies. All animal procedures were performed according to a protocol approved by the UCSF Institutional Animal Care and Use Committee (IACUC). Six-week-old female nu/nu (nude) mice weighing 18−23 g were purchased from Charles River Laboratories (Hollister, CA). For tumor inoculation, the cells were implanted in the number 4 mammary fat pad (β-estradiol pellets were also implanted subcutaneously in the flank for MCF7 clone 18 cells) or in the right flank for subcutaneous models. The imaging and biodistribution experiments were started approximately 2 weeks following implantation, when the tumors were ∼1 cm in diameter.

Tumor-bearing nude mice in sets of 3 animals per study group were injected in the tail vein (intravenous, iv) with 150−250 μCi (5.5−9.25 MBq) of ^{64}Cu-labeled MS2 conjugates in 100 μL of sterile saline. One animal from each group was selected for imaging with microPET/CT (Inveon microPET docked with microCT, Siemens Molecular Solutions, Malvern, PA). The list mode data were acquired from the time of injection to 1 h postinjection, and dynamic multiframe reconstruction was performed to capture dynamics of ^{64}Cu-labeled MS2 conjugates. In addition, a 20 min static scan was performed at 24 h postinjection. CT scans were performed after each PET scan to provide anatomical localization of radionuclide data, as well as photon attenuation map for attenuation-corrected PET reconstruction. Images were reconstructed using the AMIDE software v.1.0.4.

The dynamic images were used for determining the circulation profile of the agents by integrating the signal over a region of interest in the left ventricle of the heart (AMIDE software). The $\log_{10}$ of the integrated signal was plotted versus the midpoint of each scan frame.

Mice were sacrificed at 1 or 24 h postinjection, and the blood, tumor, and major organs were harvested and weighed. The radioactivity present in each sample was measured using a Wizard gamma counter (PerkinElmer, Waltham, MA). All values were decay corrected, and the percentage injected dose per gram (% ID/g) was calculated for each tissue sample. Means and standard deviations were calculated for each group. Using Excel software (Microsoft, Redmond, WA), an unpaired *t* test with equal variance and a two-tailed *p* value was performed for organs from different data sets. A result was considered statistically significant if it occurred at the $p < 0.05$ level.

To determine the assembly state of the agents after circulating *in vivo*, blood samples were allowed to coagulate (30 min at room temperature) and serum was collected by spinning at 10000*g* for 10 min and removing the supernatant. Serum aliquots were injected into an SEC HPLC system and the radioactivity channel was monitored for peaks corresponding to the assembled MS2 capsid, its monomer units, or ^{64}Cu associated with other serum proteins.

RESULTS AND DISCUSSION

Synthesis and Characterization of MS2−Antibody Conjugates. We first synthesized a series of MS2−antibody (MS2−Ab) conjugates (Figure 1, Supplementary Figure S1) using a recently developed oxidative coupling strategy for conjugating two macromolecules in a rapid and high-yielding reaction.[46] Control over the site for antibody attachment was attained by introducing the *p*-aminophenylalanine (*p*aF) unnatural amino acid at position 19 of the MS2 capsid proteins.[51,52] This residue is located on the exterior surface of the assembly and reacts readily with aminophenol groups in the presence of mild oxidants, as shown previously.[21,44,46] For achieving targeting, we used a humanized monoclonal antibody against the epidermal growth factor receptor (α-EGFR), although similar results were observed with the anti-human epidermal growth factor receptor (α-HER2) antibody (data not shown). The EGFR and HER2 receptors are targets of interest since they are overexpressed in numerous types of cancer, such as breast cancer, glioma, and colon cancer.[53−55]

We explored the use of linkers between the viral capsids and the antibodies (Figure 1) to allow for efficient interaction of the antibody with the receptor targeted. Flow cytometry experiments (*vide infra*, Supplementary Figure S2) suggest that the length of the linker (two carbon atoms, or polyethylene glycol with molecular weights of 2 kDa or 5 kDa) did not affect the affinity of the antibody to its target. The PEG chain, however,

DOI: 10.1021/acs.molpharmaceut.6b00566
Mol. Pharmaceutics 2016, 13, 3764−3772

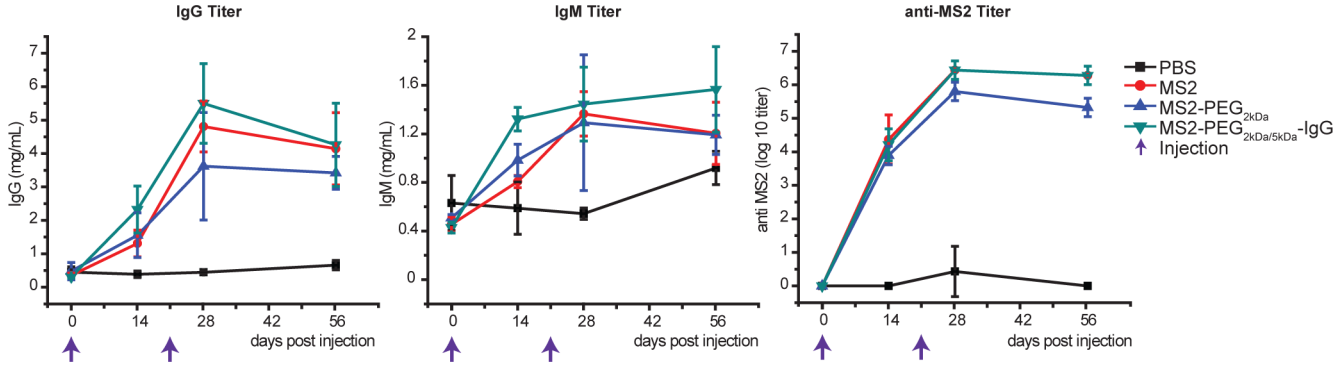

Figure 2. Immunogenicity assay. The amount of IgG, IgM, and anti-MS2 coat protein antibodies in the serum of Balb/c mice was measured at different time points postinjection using ELISA assays. Although the amount of antibodies produced for all of the MS2 samples was statistically higher than the PBS negative control (black line), the differences between the agents were not significant (unpaired *t* test with equal variance and a two-tailed *p* value, $p > 0.05$).

could have a shielding effect from the immune system and therefore was used in most *in vivo* experiments. We also explored constructs with a small number of antibodies linked to the MS2 capsids through $PEG_{5\ kDa}$ linkers and additional surface coating with PEG_{2kDa} (i.e., "backfilling" via a subsequent oxidative coupling reaction) in order to shield the surface of the viral capsid while still allowing the antibodies to interact unobstructedly with their targets.[56]

Dynamic light scattering (DLS) and transmission electron microscopy (TEM) studies (Supplementary Figure S1) suggested homogeneous populations of MS2 derivatives, with the hydrodynamic radii increasing from 27 to 30.7 nm upon conjugation of antibodies, and to 28.9 nm when PEG_{5kDa} was used as a linker. In the backfilling case, the measured diameter was 33.7 nm. We hypothesize that, when the two carbon linker is used, the antibodies are attached tangentially to the capsid surface, explaining the relatively small increase in diameter. Given the surface of the MS2 bacteriophage (~2300 nm^2) and the number of PEG chains attached (100−130 per capsid), the density of PEG chains is likely insufficient to extend the polymers to the "brush" conformations.[57,58] This expectation is supported by the fact that the predicted length of the fully extended PEG chain is ~16 nm for PEG_{2kDa} and ~35 nm for PEG_{5kDa},[59] but only small increases in nanoparticle diameter are observed by DLS.

***In Vitro* Interactions with Cancer Cell Models.** Fluorescently labeled MS2 conjugates were used in flow cytometry and confocal microscopy experiments to investigate their interaction with breast cancer cell lines. These samples were prepared by reacting cysteine residues introduced at position 87 with Oregon Green 488 (OG488) maleimide dyes, as shown in Supplementary Figure S2a. Mass spectrometry analysis shows that near-complete modifications can be obtained, resulting in agents with more than 100 copies of the small molecule attached. Subsequent incubation of these samples with two breast cancer cell lines indicated that the targeted agents have specific interactions with surface receptors of interest (Supplementary Figure S2b). The addition of PEG linkers to extend the antibody further from the capsid surface did not seem to improve the binding to the targeted receptor (Supplementary Figure S2c). Flow cytometry experiments (Supplementary Figure S2d) did not reveal any clear advantage of having more than 3 copies of the antibody per capsid, and thus for cost efficiency, conjugates with three or fewer copies of antibodies were used for all subsequent studies. Preincubation of the agents in mouse serum did not inhibit their ability to bind the cells (Supplementary Figure S2e), suggesting that serum proteins are not detrimental to the binding of the MS2−Ab conjugates.[56]

Live-cell confocal microscopy with these agents confirms that the binding is specific to the cells expressing the targeted receptor (Supplementary Figure S3). HCC1954 cells were incubated for 1 h at 37 °C with OG488-labeled MS2, MS2−αEGFR, and MS2-PEG_{5kDa}-αEGFR in DPBS with 1% FBS. Fluorescent signal was observed on the cell surfaces and, at later time points, inside the cells, in several vesicles. These results indicate that, upon binding to the surface receptors, the constructs are internalized.

***In Vivo* Assessment of Immunogenicity of MS2−Ab Conjugates.** Balb/c mice with intact immune systems were administered MS2-based agents through tail vein injection in two doses, at $t = 0$ and 3 weeks. The agents tested were MS2, MS2 coated with ~130 strands of methoxy-terminated PEG_{2kDa} (MS2-PEG_{2kDa}), and MS2 decorated with both antibodies with PEG_{5kDa} spacers and PEG_{2kDa} backfilling (MS2-$PEG_{2kDa/5kDa}$-IgG). To facilitate the ability to distinguish the immune response caused by the capsids from the immunogenicity of the humanized anti-EGFR antibody, a mouse IgG antibody was used for this study.

After the first dose, the amount of total IgM and IgG produced by animal groups treated with the three agents was similar (0.5−2 mg/mL). Upon injection of the second dose, the amount of IgG produced was 3−4 times higher than the IgM (Figure 2). Brown et al.[24] observed a similar ratio of IgG to IgM antibodies, indicating that, upon multiple administrations of MS2 (albeit subcutaneous in their case), the bulk of the response was in the form of IgG.

Anti-MS2 coat protein antibodies were present in the serum after the initial dosing, and a small increase was observed after the second dose (Figure 2). Using a two sample unpaired Student *t* test, we determined that the amounts of antibodies produced upon injection of the MS2 agents were significantly higher ($p < 0.05$) than the PBS control. The addition of PEG chains did not seem to have a significant effect on the amount of antibody produced. This phenomenon might be explained by the fact that even if there are about 130 strands of PEG per capsid, they might not reach the "brush regime"[57] and could be less efficient at shielding the viral capsid from the immune system.[39] Mastico et al.[60] have also observed the production of anti-MS2 antibodies in mice, which was amplified by the

DOI: 10.1021/acs.molpharmaceut.6b00566
Mol. Pharmaceutics 2016, 13, 3764−3772

addition of a nonapeptide derived from hemagglutinin. Although there is a paucity of studies on the immune response caused by iv administration of viral capsids as delivery agents (and not as vaccines), a study by Kaiser et al.[36] noted that antibody production against CCMV and Hsp was also observed.

Radiolabeling of MS2 Capsids. In biomedical imaging applications based on radioactivity, the radionuclide itself is detected rather than the nanoparticle or the payload. Therefore, the radiolabeling strategy must involve a stable interaction between the tracer and the carrier. Additionally, the radionuclide half-life has to be compatible with the *in vivo* pharmacokinetics of the probe. In recent years, copper-64 (^{64}Cu) has attracted increasing attention as a promising radionuclide due to its decay characteristics (half-life $t_{1/2}$ = 12.7 h) that are compatible with the time scales required for the biodistribution of agents, such as monoclonal antibodies and nanoparticles that exhibit long circulation times. Radiolabeling of systems of interest can be obtained by coordination with ligands such as 1,4,7,10-tetraazacyclododecane-1,4,7,10-tetraacetic acid (DOTA) or 2,2′,2″-(1,4,7-triazonane-1,4,7-triyl)-triacetic acid (NOTA). These ligands utilize both the macrocyclic and chelate effects to enhance the stability of the chelator−isotope construct.[61]

The radiolabeling of MS2 conjugates was accomplished by incubating the ^{64}Cu in its chloride form with MS2 capsids modified by reacting chelators (*vide infra*) bearing a maleimide moiety with internal cysteine residues. Up to 180 copies of the chelators were installed on the interior surface of each capsid, leading to an increased load of isotopes inside the VLP (Supplementary Figure S4). Housing the radioisotope inside the capsid also mitigates the ability of the ^{64}Cu to interact with serum proteins and escape from the carrier. Upon desalting and concentrating steps to remove excess radioisotope, radiochemical yields between 65 and 85% were obtained. The total synthesis time was between 3 and 4 h, leading to >95% pure radiolabeled capsids, as verified by high performance liquid chromatography size exclusion chromatography (SEC HPLC, Supplementary Figure S5). Compared to other approaches to radiolabeling nanoparticles, this strategy is more facile and requires fewer steps.

***In Vitro* and *in Vivo* Stability of MS2−Ab Conjugates.** We tested 4 possible chelators (NOTA, NOTA-GA, DOTA, and DOTA-GA) to compare the stability of the complexes they form with the ^{64}Cu radioisotope ions. Similar stability was observed for all the chelators investigated, with NOTA showing a larger amount of signal associated with the intact capsid peak at longer time points. Based on these results, we decided to proceed with the NOTA−MS2 conjugates for *in vivo* experiments.

Radiolabeled conjugates were analyzed for purity and assembly state using SEC HPLC. The radioactivity traces indicated that most of the radioactive ^{64}Cu isotope remained associated with the intact capsids even upon incubation in mouse serum at physiological temperature (Figure 3, Supplementary Figure S5) or after circulating *in vivo* for 24 h (Supplementary Figure S6). Similar results were observed upon incubation in PBS alone (data not shown). MS2−antibody conjugates showed excellent stability at 37 °C (Supplementary Figure S7). This high level of intact capsid is encouraging for drug delivery applications, for which it is important to allow enough time for specific accumulation in the region of interest before releasing the active molecule. By housing the cargo on the inside of the capsid, the side effects of systemic administration of chemotherapeutics could be mitigated. The second peak (shoulder at retention time ∼6.3 min, Supplementary Figures S5, S6, and S7) can be attributed to the dissociation of ^{64}Cu from the chelator and nonspecific interactions with other serum proteins or to the partial disassembly of the MS2 capsids. Importantly, to allow for the capsids to be cleared from circulation, a gradual degradation is desired.

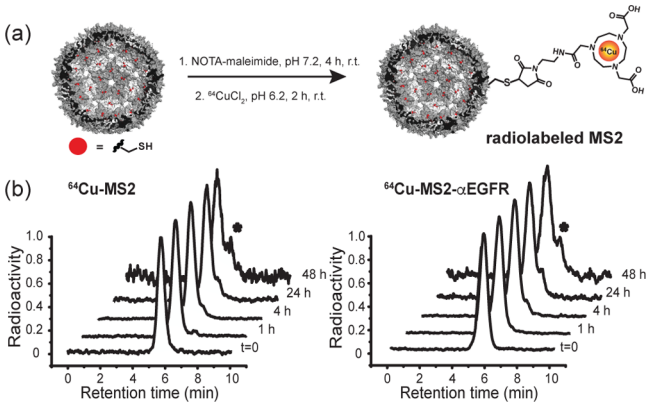

Figure 3. (a) Synthetic scheme for radiolabeling MS2 bacteriophage using the internal Cys residues (cutaway view). (b) Stability of MS2−NOTA-^{64}Cu and radiolabeled MS2−antibody conjugate in mouse serum. The normalized signal from the radioactivity channel during SEC HPLC runs of aliquots taken at time points from 0 to 48 h indicates that the predominant species is the ^{64}Cu-labeled intact MS2 capsid. The secondary peak (*) is likely due to partial disassembly or loss of ^{64}Cu and its interaction with other serum proteins.

Positron Emission Tomography. Several molecular imaging approaches have been used for tracking the distribution of agents with therapeutic potential, including positron emission tomography (PET), single photon emission computed tomography (SPECT), magnetic resonance imaging (MRI), computed tomography (CT), ultrasound, bioluminescence, and fluorescence imaging.[62] Radionuclide-based imaging methods, especially PET, have been a particular focus in biomedical research due to advantages such as high sensitivity (picomolar level) and excellent tissue penetration by the signal.[63] Currently, most PET radiopharmaceuticals are based on small molecules, but their rapid clearance and poor specificity to tissues of interest are common drawbacks. In contrast, nanoparticles can have longer residence time in the body and possess sites that can be used for derivatization with radionuclides and targeting moieties. In addition, they have the potential to attain high specific activity (amount of radioactivity per mass of carrier), which is extremely important in order to achieve high-quality images at low doses of radioactivity. For our system, the specific activity was on average 1.1 GBq/mg capsid, as compared to 0.37−0.74 GBq/mg Fe reported for ^{64}Cu-DOTA−iron oxide nanoparticles,[63] and 15 GBq/mg reported for polymer nanoparticles.[63]

We used PET as a noninvasive way to gain information about the biodistribution of the MS2 conjugates in real time and at different time points while limiting the number of animals used. Dynamic imaging was performed from the time of injection until 1 h postinjection, and a 20 min static scan was collected at 24 h postinjection (Figure 4a,b).

The dynamic PET images taken from time of injection to 1 h postinjection were used to determine the clearance profile of

DOI: 10.1021/acs.molpharmaceut.6b00566
Mol. Pharmaceutics 2016, 13, 3764−3772

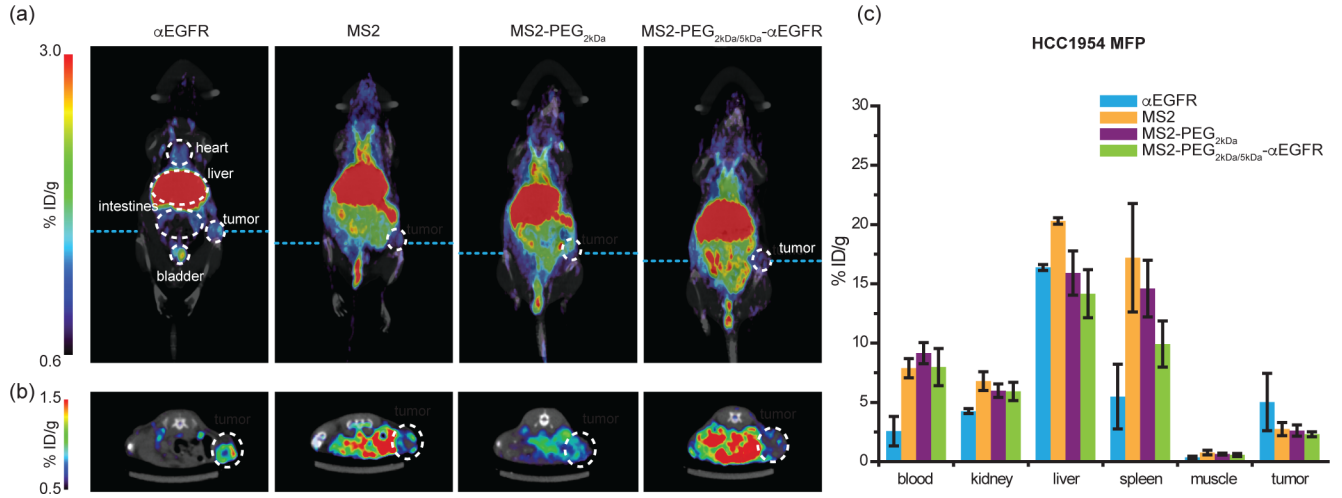

Figure 4. *In vivo* distribution of ^{64}Cu-labeled MS2 scaffolds in nude mice with HCC1954 orthotopic breast cancer tumors (mammary fat pad, MFP). Mice were injected with 150−250 μCi radiolabeled agents. ^{64}Cu-labeled antibodies were used as positive controls. (a) PET scans were acquired at 24 h postinjection. A maximum intensity projection (MIP) of the PET signal within a 50 mm slice is presented overlaid with a CT slice of 1 mm from the coronal plane. The horizontal blue dashed line represents the slice used for the transverse plane image in panel b. (b) A transverse plane through the tumor is shown to illustrate the agent distribution within the tumor. (c) Biodistribution studies were performed 24 h postinjection by harvesting the major organs, measuring their radioactivity using a scintillation counter and normalizing the radioactivity by the mass of the tissue. The error bars represent the standard deviation from triplicate samples.

the injected agents. A 3D region of interest (ROI) was chosen to overlap with the left ventricle of the heart to estimate the radioactivity present in the blood pool.[64] The signal showed a decay profile corresponding to a two compartment model, as evidenced by the shape of the of the $\log_{10}$ plot of the signal within the ROI against the midpoint of each scanning frame (Supplementary Figure S9). The breathing motion and the heartbeat of the mouse, as well as the limited resolution of the animal scale PET scanner, made it difficult to determine the precise half-lives of the agents. However, the small slope of the curve at later time points (elimination phase) indicates a slow clearance for all agents. Surprisingly, no significant increase in circulation half-life was attained after PEG or antibody modification. The antibody had a shorter half-life than expected, which could be due to multiple modifications with the chelator leading to an altered clearance, or to dissociation of the ^{64}Cu from the chelator.[65,66]

Throughout the experiment, a significant amount of signal was observed in the liver, the lower abdominal area, and the heart. Based on the signal in the heart and the biodistribution results, we concluded that the unmodified MS2 capsid and its derivatives remain in circulation for a prolonged time. At 24 h postinjection, the decay-corrected signal was significantly weaker overall, as result of the agents being cleared from the system (Figure 4a,b).

Biodistribution Studies. Mice were injected with each agent and sacrificed at either 1 or 24 h time points. The blood and major organs were harvested, and their activity was measured using a gamma counter. The tissue samples were weighed, and the radioactivity signal was normalized as percent injected dose per gram of tissue (% ID/g, Figure 4c and Supplementary Figure S9). To investigate the nonspecific tissue uptake of the agents, we calculated the tumor-to-muscle ratios by dividing the % ID/g in the tumor by the signal from the muscle tissue (Table 1). The numbers greater than 1 indicate specific uptake of the agents into the tumor. The free anti-EGFR antibody used as positive control had the highest tumor-to-muscle ratio. Notably, the amount of antibody injected was

Table 1. Tumor-to-Muscle Ratio (T/M) of the Normalized Radioactive Signal per Unit Weight (% ID/g) Calculated as a Measure of Nonspecific Accumulation of the Agents[a]

	T/M	
agent	MFP	SC
αEGFR	14.25 ± 5.71	23.83 ± 12.12
MS2	3.70 ± 1.04	2.55 ± 1.63
MS2-PEG$_{2kDa}$	4.18 ± 1.09	3.52 ± 1.79
MS2-PEG$_{2kDa/5kDa}$-αEGFR	4.62 ± 1.26	4.91 ± 2.72

[a]T/M = 1 indicates no specificity for the tumor over the muscle.

3−4 times more than the equivalent amount of antibodies attached to the MS2 capsids. In parallel studies (Supplementary Figure S10), we observed higher uptake of the free antibody control modified using the same protocol. However, the uptake of MS2 agents was very similar. The MS2 agents had tumor-to-muscle ratios in the range of 2.5−4.9, indicating specific uptake in the tumor compared to muscle tissue (Table 1). Overall tumor uptake for the MS2-based agents varied between 2 and 5% ID/g at 24 h postinjection (Figure 4c). The tissues with the largest degree of accumulation were the liver, the spleen (the usual clearance pathways for nanoparticles[67]), and the large intestine. The high signals in the blood even after 24 h of circulation validate the long half-lives observed from the analysis of the dynamic PET scans.

At 24 h postinjection, a similar amount of activity is present in the tumor for both the targeted and the untargeted viral capsids, suggesting that the extravasation from the blood vessel to the tumor might be the limiting step. Some recent studies have shown that a spherical structure is not ideal for crossing the gaps in the endothelial cell layer of tumor blood vessels.[31,68] Our results also indicate that targeting does not provide a significant improvement in the efficiency of the agent to accumulate in the region of interest, which has also been noted in the case of gold nanoparticles of similar size.[17,69,70] Similar results were observed in the case of liposomes,[71] although further studies investigating the delivery of drug molecules

DOI: 10.1021/acs.molpharmaceut.6b00566
Mol. Pharmaceutics 2016, 13, 3764−3772

indicated a clear benefit to the attachment of the targeting moiety,[72] presumably due to increased uptake once the cancer cells were reached.

The work presented herein is one of the few examples of antibody-targeted protein-based nanoparticles to be investigated for tumor homing. The particles exhibit surprisingly long circulation profiles and accumulate within the tumor environment. However, no significant difference is observed between the targeted and untargeted viral capsids, indicating that the diffusion through the endothelial gaps might be the limiting factor in determining tumor accumulation of nanoparticles. Our observations add evidence to the case that other factors, such as size, shape, and overall charge, might play a bigger role in the homing of nanoparticles to the tumor, while the targeting groups can increase specificity to tumor cells within the tumor environment. This hypothesis can help guide the design of nanoparticle carriers with various physical properties, while the synthetic plan and battery of analyses performed in this work can provide a framework for the thorough characterization of new scaffolds for drug delivery.

CONCLUSIONS

In vitro results indicate specific binding of the MS2−Ab targeted agents to the EGFR receptor on the surface of cancer cell models. The agents can be radiolabeled to obtain high-specific-activity constructs that maintain structural integrity over 48 h when incubated in mouse serum at 37 °C. Upon intravenous injection in mouse breast cancer models, the MS2 viral capsid conjugates show moderate tumor uptake, comparable to targeted inorganic nanoparticles. No significant difference in tumor uptake is observed between the antibody-targeted and untargeted capsids.

Given the potential of the MS2 VLPs to carry up to 180 copies of drug molecule cargo, the large amount of agent accumulated in the tumor could provide a significant therapeutic effect. As such, the efficiency of MS2−antibody conjugates for delivering drug cargo and inhibiting tumor growth will be investigated. Recent studies have investigated the effects of size and shape of the carrier on the accumulation of the nanoparticle in the tumor.[31] Comparison studies with other virus-like particle shapes available (such as disks and rods) for their ability to deliver cargo to tumor environments are currently underway in our laboratory.

In this study, we have shown that MS2 is a robust and synthetically versatile platform that has a slow clearance profile *in vivo*. *In vitro* results suggest that the MS2 platform remains an attractive candidate for the synthesis of targeted agents for a variety of diseases. However, based on the limited tumor uptake *in vivo*, the targeting functionalities appended to these capsids might have to focus on disease targets that do not require extravasation, such as the treatment and monitoring of cardiovascular diseases and liquid tumors.

ASSOCIATED CONTENT

Supporting Information

The Supporting Information is available free of charge on the ACS Publications website at DOI: 10.1021/acs.molpharmaceut.6b00566.

Synthetic schemes, agent characterization, flow cytometry experiments, live-cell microscopy, stability studies, and additional biodistribution experiments (PDF)

AUTHOR INFORMATION

Corresponding Author

*Department of Chemistry, University of California, Berkeley, 724 Latimer Hall, Berkeley, CA 94720, United States. Phone: (510) 643-9915. E-mail: mbfrancis@berkeley.edu.

Notes

The authors declare no competing financial interest.

ACKNOWLEDGMENTS

The antibody modification studies were funded by the DOD Breast Cancer Research Program (Grants BC061995 and W81XWH-14-0400) and the W. M. Keck Foundation. I.L.A. was supported by a Genentech Fellowship through the U.C. Berkeley Chemical Biology program. M.E.F. was supported by DOD BCRP Grant BC100159. C.N. was supported by a Howard Hughes Medical Institute International Student Research Fellowship. LCMS instrumentation was acquired with National Institutes of Health Grant 1S10RR022393-01. The PET/CT scanner was acquired using the NIH grant S10 RR023051. We are grateful to the Preclinical Therapeutics Core at UCSF for generating the tumor models used in this study.

ABBREVIATIONS USED

EGFR, epidermal growth factor receptor; PET, positron emission tomography; PEG, polyethylene glycol

REFERENCES

(1) Winnard, P. T., Jr.; Pathak, A. P.; Dhara, S.; Cho, S. Y.; Raman, V.; Pomper, M. G. Molecular Imaging of Metastatic Potential. *J. Nucl. Med.* **2008**, *49*, 96S−112S.

(2) Aslam, M. S.; Naveed, S.; Ahmed, A.; Abbas, Z.; Gull, I.; Athar, M. A. Side Effects of Chemotherapy in Cancer Patients and Evaluations of Patients Opinion about Starvation Based Differential Chemotherapy. *J. Cancer Ther.* **2014**, *5*, 817−822.

(3) Liu, S.; Maheshwari, R.; Kiick, K. L. Polymer-Based Therapeutics. *Macromolecules* **2009**, *42*, 3−13.

(4) Svenson, S.; Tomalia, D. A. Dendrimers in Biomedical Applications − Reflections on the Field. *Adv. Drug Delivery Rev.* **2005**, *57*, 2106−2129.

(5) Lee, C. C.; MacKay, J. A.; Fréchet, J. M. J.; Szoka, F. C. Designing Dendrimers for Biological Applications. *Nat. Biotechnol.* **2005**, *23*, 1517−1526.

(6) Torchilin, V. P. Recent Advances with Liposomes as Pharmaceutical Carriers. *Nat. Rev. Drug Discovery* **2005**, *4*, 145−160.

(7) Tiwari, G.; Tiwari, R.; Sriwastawa, B.; Bhati, L.; Pandey, S.; Pandey, P.; Bannerjee, S. K. D. Drug Delivery Systems: An Updated Review. *Int. J. Pharm. Investig.* **2012**, *2*, 2−11.

(8) Steinmetz, N. F. Viral Nanoparticles as Platforms for Next Generation Therapeutics and Imaging Devices. *Nanomedicine* **2010**, *6*, 634−641.

(9) Yildiz, I.; Shukla, S.; Steinmetz, N. F. Applications of Viral Nanoparticles in Medicine. *Curr. Opin. Biotechnol.* **2011**, *22*, 901−908.

(10) Prasuhn, D. E., Jr.; Singh, P.; Strable, E.; Brown, S.; Manchester, M.; Finn, M. G. Plasma Clearance of Bacteriophage Qβ as a Function of Surface Charge. *J. Am. Chem. Soc.* **2008**, *130*, 1328−1334.

(11) Gerlowski, L. E.; Jain, R. K. Microvascular Permeability of Normal and Neoplastic Tissues. *Microvasc. Res.* **1986**, *31*, 288−305.

(12) Dreher, M. R.; Liu, W.; Michelich, C. R.; Dewhirst, M. W.; Yuan, F.; Chilkoti, A. Tumor Vascular Permeability, Accumulation, and Penetration of Macromolecular Drug Carriers. *J. Natl. Cancer Inst.* **2006**, *98*, 335−334.

(13) Maeda, H.; Wu, J.; Sawa, T.; Matsumura, Y.; Hori, K. Vascular Permeability and the EPR Effect in Macromolecular Therapeutics: A Review. *J. Controlled Release* **2000**, *65*, 271−284.

DOI: 10.1021/acs.molpharmaceut.6b00566
Mol. Pharmaceutics 2016, 13, 3764−3772

(14) Bertrand, N.; Wu, J.; Xu, X.; Kamaly, N.; Farokhzad, O. C. Cancer Nanotechnology: The Impact of Passive and Active Targeting in the Era of Modern Cancer Biology. *Adv. Drug Delivery Rev.* **2014**, *66*, 2−25.
(15) Yuan, F.; Dellian, M.; Fukumura, D.; Leunig, M.; Berk, D. A.; Torchilin, V. P.; Jain, R. K. Vascular Permeability in a Human Tumor Xenograft: Molecular Size. *Cancer Res.* **1995**, *55*, 33752−33756.
(16) Leu, A. J.; Berk, D. A.; Lyumboussaki, A.; Alitalo, K.; Jain, R. K. Absence of Functional Lymphatics within a Murine Sarcoma: A Molecular and Functional Evaluation. *Cancer Res.* **2000**, *60*, 4324−4327.
(17) Wittrup, K. D.; Thurber, G. M.; Schmidt, M. M.; Rhoden, J. J. Practical Theoretic Guidance for the Design of Tumor-Targeting Agents. In *Methods in Enzymology*, 1st ed.; Wittrup, K. D., Verdine, G. L., Eds.; Elsevier: Cambridge, 2012; Vol. *503*, pp 56−268.
(18) Destito, G.; Yeh, R.; Rae, C. S.; Finn, M. G.; Manchester, M. Folic Acid-Mediated Targeting of Cowpea Mosaic Virus Particles to Tumor Cells. *Chem. Biol.* **2007**, *14*, 1152−1162.
(19) Ren, Y.; Wong, S. M.; Lim, L. Y. Folic Acid Conjugated Protein Cages of a Plant Virus: A Novel Delivery Platform for Doxorubicin. *Bioconjugate Chem.* **2007**, *18*, 836−843.
(20) Tong, G. J.; Hsiao, S. C.; Carrico, Z. M.; Francis, M. B. Viral Capsid DNA Aptamer Conjugates as Multivalent Cell Targeting Vehicles. *J. Am. Chem. Soc.* **2009**, *131*, 11174−11178.
(21) Behrens, C. R.; Hooker, J. M.; Obermeyer, A. C.; Romanini, D. W.; Katz, E. M.; Francis, M. B. Rapid Chemoselective Bioconjugation Through the Oxidative Coupling of Anilines and Aminophenols. *J. Am. Chem. Soc.* **2011**, *133*, 16398−16401.
(22) Hovlid, M. L.; Steinmetz, N. F.; Laufer, B.; Lau, J. L.; Kuzelka, J.; Wang, Q.; Hyypiä, T.; Nemerow, G. R.; Kessler, H.; Manchester, M.; Finn, M. G. Guiding Plant Virus Particles to Integrin-Displaying Cells. *Nanoscale* **2012**, *4*, 3698−3705.
(23) Rhee, J. K.; Baksh, M.; Nycholat, C.; Paulson, J. C.; Kitagishi, H.; Finn, M. G. Glycan-Targeted Virus-Like Nanoparticles for Photodynamic Therapy. *Biomacromolecules* **2012**, *13*, 2333−2338.
(24) Brown, W. L.; Mastico, R. A.; Wu, M.; Heal, K. G.; Adams, C. J.; Murray, J. B.; Simpson, J. C.; Lord, J. M.; Taylor-Robinson, A. W.; Stockley, P. G. RNA Bacteriophage Capsid-Mediated Drug Delivery and Epitope Presentation. *Intervirology* **2002**, *45*, 371−380.
(25) Fiandra, L.; Mazzucchelli, S.; De Palma, C.; Colombo, M.; Allevi, R.; Sommaruga, S.; Clementi, E.; Bellini, M.; Prosperi, D.; Corsi, F. Assessing the *In Vivo* Targeting Efficiency of Multifunctional Nanoconstructs Bearing Antibody-Derived Ligands. *ACS Nano* **2013**, *7*, 6092−6102.
(26) Flenniken, M. L. *Protein Cage Architectures For Targeted Therapeutic And Imaging Agent Delivery*. Ph.D. Thesis, Montana State University: July 2006.
(27) Sapra, P.; Shor, B. Monoclonal Antibody-Based Therapies in Cancer: Advances and Challenges. *Pharmacol. Ther.* **2013**, *138*, 452−469.
(28) Paszko, E.; Senge, M. O. Immunoliposomes. *Curr. Med. Chem.* **2012**, *19*, 5239−5277.
(29) Singh, P.; Gonzalez, M. J.; Manchester, M. Viruses and Their Uses in Nanotechnology. *Drug Dev. Res.* **2006**, *67*, 23−41.
(30) Molino, N. M.; Wang, S. W. Caged Protein Nanoparticles for Drug Delivery. *Curr. Opin. Biotechnol.* **2014**, *28*, 75−82.
(31) Albanese, A.; Tang, P. S.; Chan, W. C. W. The Effect of Nanoparticle Size, Shape, and Surface Chemistry on Biological Systems. *Annu. Rev. Biomed. Eng.* **2012**, *14*, 1−16.
(32) Longmire, M.; Choyke, P. L.; Kobayashi, H. Clearance Properties of Nano-sized Particles and Molecules as Imaging Agents: Considerations and Caveats. *Nanomedicine (London, U. K.)* **2008**, *3*, 703−717.
(33) Rae, C. S.; Khor, I. W.; Wang, Q.; Destito, G.; Gonzalez, M. J.; Singh, P.; Thomas, D. M.; Estrada, M. N.; Powell, E.; Finn, M. G.; Manchester, M. Systemic Trafficking of Plant Virus Nanoparticles in Mice via the Oral Route. *Virology* **2005**, *343*, 224−235.
(34) Singh, P.; Prasuhn, D.; Yeh, R. M.; Destito, G.; Rae, C. S.; Osborn, K.; Finn, M. G.; Manchester, M. Biodistribution, Toxicity, and Pathology of Cowpea Mosaic Virus Nanoparticles. *J. Controlled Release* **2007**, *120*, 41−50.
(35) Shukla, S.; Wen, A. M.; Ayat, N. R.; Commandeur, U.; Gopalkrishnan, R.; Broome, A. M.; Lozada, K. W.; Keri, R. A.; Steinmetz, N. F. Biodistribution and Clearance of a Filamentous Plant Virus in Healthy and Tumor-Bearing Mice. *Nanomedicine (London, U. K.)* **2014**, *9*, 221−235.
(36) Kaiser, C. R.; Flenniken, M. L.; Gillitzer, E.; Harmsen, A. L.; Harmsen, A. G.; Jutila, M. A.; Douglas, T.; Young, M. J. Biodistribution Studies of Protein Cage Nanoparticles Demonstrate Broad Tissue Distribution and Rapid Clearance *In Vivo*. *Int. J. Nanomed.* **2007**, *2*, 715−733.
(37) Storm, G.; Belliot, S. O.; Daemen, T.; Lasic, D. D. Surface Modification of Nanoparticles to Oppose Uptake by the Mononuclear Phagocyte System. *Adv. Drug Delivery Rev.* **1995**, *17*, 31−48.
(38) Raja, K. S.; Wang, Q.; Gonzalez, M. J.; Manchester, M.; Johnson, J. E.; Finn, M. G. Hybrid Virus-Polymer Materials. 1. Synthesis and Properties of PEG-Decorated Cowpea Mosaic Virus. *Biomacromolecules* **2003**, *4*, 472−476.
(39) Kovacs, E. W.; Hooker, J. M.; Romanini, D. W.; Holder, P. G.; Berry, K. E.; Francis, M. B. Dual-Surface-Modified Bacteriophage MS2 as an Ideal Scaffold for a Viral Capsid-Based Drug Delivery System. *Bioconjugate Chem.* **2007**, *18*, 1140−1147.
(40) O'Riordan, C. R.; Lachapelle, A.; Delgado, C.; Parkes, V.; Wadsworth, S. C.; Smith, A. E.; Francis, G. E. PEGylation of Adenovirus with Retention of Infectivity and Protection from Neutralizing Antibody *In Vitro* and *In Vivo*. *Hum. Gene Ther.* **1999**, *10*, 1349−1358.
(41) Caliceti, P.; Veronese, F. M. Pharmacokinetic and Biodistribution Properties of Poly(Ethylene Glycol)-Protein Conjugates. *Adv. Drug Delivery Rev.* **2003**, *55*, 1261−1277.
(42) van Kan-Davelaar, H. E.; van Hest, J. C. M.; Cornelissen, J. J. L. M.; Koay, M. S. T. Using Viruses as Nanomedicines. *Br. J. Pharmacol.* **2014**, *171*, 4001−4009.
(43) Carrico, Z. M.; Romanini, D. W.; Mehl, R. A.; Francis, M. B. Oxidative Coupling of Peptides to a Virus Capsid Containing Unnatural Amino Acids. *Chem. Commun.* **2008**, 1205−1207.
(44) Hooker, J. M.; Esser-Kahn, A. P.; Francis, M. B. Modification of Aniline Containing Proteins Using an Oxidative Coupling Strategy. *J. Am. Chem. Soc.* **2006**, *128*, 15558−15559.
(45) Stephanopoulos, N.; Tong, G. J.; Hsiao, S. C.; Francis, M. B. Dual-Surface Modified Virus Capsids for Targeted Delivery of Photodynamic Agents to Cancer Cells. *ACS Nano* **2010**, *4*, 6014−6020.
(46) ElSohly, A. M.; Netirojjanakul, C.; Aanei, I. L.; Jager, A.; Bendall, S. C.; Farkas, M. E.; Nolan, G. P.; Francis, M. B. Synthetically Modified Viral Capsids as Versatile Carriers for Use in Antibody-Based Cell Targeting. *Bioconjugate Chem.* **2015**, *26*, 1590−1596.
(47) Wu, W.; Hsiao, S. C.; Carrico, Z. M.; Francis, M. B. Genome-Free Viral Capsids as Multivalent Carriers for Taxol Delivery. *Angew. Chem., Int. Ed.* **2009**, *48*, 9493−9497.
(48) Garimella, P. D.; Datta, A.; Romanini, D. W.; Raymond, K. N.; Francis, M. B. Multivalent, High-relaxivity MRI Contrast Agents Using Rigid Cysteine-Reactive Gadolinium Complexes. *J. Am. Chem. Soc.* **2011**, *133*, 14704−14709.
(49) Farkas, M. E.; Aanei, I. L.; Behrens, C. R.; Tong, G. J.; Murphy, S. T.; O'Neil, J. P.; Francis, M. B. PET Imaging and Biodistribution of Chemically Modified Bacteriophage MS2. *Mol. Pharmaceutics* **2013**, *10*, 69−76.
(50) Ashley, C. E.; Carnes, E. C.; Phillips, G. K.; Durfee, P. N.; Buley, M. D.; Lino, C. A.; Padilla, D. P.; Phillips, B.; Carter, M. B.; Willman, C. L.; Brinker, C. J.; Caldeira, J. d. C.; Chackerian, B.; Wharton, W.; Peabody, D. S. Cell-Specific Delivery of Diverse Cargos by Bacteriophage MS2 Virus-like Particles. *ACS Nano* **2011**, *5*, 5729−5745.
(51) Mehl, R. A.; Anderson, J. C.; Santoro, S. W.; Wang, L.; Martin, A. B.; King, D. S.; Horn, D. M.; Schultz, P. G. Generation of a Bacterium with a 21 Amino Acid Genetic Code. *J. Am. Chem. Soc.* **2003**, *125*, 935−939.

DOI: 10.1021/acs.molpharmaceut.6b00566
Mol. Pharmaceutics 2016, 13, 3764−3772

(52) Xie, J.; Schultz, P. G. A Chemical Toolkit for Proteins−An Expanded Genetic Code. *Nat. Rev. Mol. Cell Biol.* **2006**, *7*, 775−782.
(53) Cheng, Z.; Al Zaki, A.; Hui, J. Z.; Muzykantov, V. R.; Tsourkas, A. Multifunctional Nanoparticles: Cost Versus Benefit of Adding Targeting and Imaging Capabilities. *Science* **2012**, *338*, 903−909.
(54) Howe, L. R.; Brown, P. H. Targeting the HER/EGFR/ErB Family to Prevent Breast Cancer. *Cancer Prev. Res.* **2011**, *4*, 1149−1157.
(55) Patel, D.; Lahiji, A.; Patel, S.; Franklin, M.; Jimenez, X.; Hicklin, D. J.; Kang, X. Monoclonal Antibody Cetuximab Binds to and Down-Regulates Constitutively Activated Epidermal Growth Factor Receptor vIII on the Cell Surface. *Anticancer Res.* **2007**, *27*, 3355−3366.
(56) Dai, Q.; Walkey, C.; Chan, W. C. W. Polyethylene Glycol Backfilling Mitigates the Negative Impact of the Protein Corona on Nanoparticle Cell Targeting. *Angew. Chem., Int. Ed.* **2014**, *53*, 1−5.
(57) Steinmetz, N. F.; Manchester, M. PEGylated Viral Nanoparticles for Biomedicine: The Impact of PEG Chain Length on VNP Cell Interactions *In Vitro* and *Ex Vivo*. *Biomacromolecules* **2009**, *10*, 784−792.
(58) Wang, M.; Thanou, M. Targeting Nanoparticles to Cancer. *Pharmacol. Res.* **2010**, *62*, 90−99.
(59) Jokerst, J. V.; Lobovkina, T.; Zare, R. N.; Gambhir, S. S. Nanoparticle PEGylation for Imaging and Therapy. *Nanomedicine (London, U. K.)* **2011**, *6*, 715−728.
(60) Mastico, R. A.; Talbot, S. J.; Stockley, P. G. Multiple Presentation of Foreign Peptides on the Surface of an RNA-free Spherical Bacteriophage Capsid. *J. Gen. Virol.* **1993**, *74*, 541−548.
(61) Dearling, J. L. J.; Voss, S. V.; Dunning, P.; Snay, E.; Fahey, F.; Smith, S. V.; Huston, J. S.; Meares, C. F.; Treves, S. T.; Packard, A. B. Imaging Cancer Using PET - the Effect of the Bifunctional Chelator on the Biodistribution of a ^{64}Cu-labeled Antibody. *Nucl. Med. Biol.* **2011**, *38*, 29−38.
(62) de Jong, M.; Essers, J.; van Weerden, W. M. Imaging Preclinical Tumour Models: Improving Translational Power. *Nat. Rev. Cancer* **2014**, *14*, 481−493.
(63) Liu, Y.; Welch, M. J. Nanoparticles Labeled with Positron Emitting Nuclides: Advantages, Methods and Applications. *Bioconjugate Chem.* **2012**, *23*, 671−682.
(64) Tantawy, M. N.; Peterson, T. E. Simplified [^{18}F]FDG Image-Derived Input Function Using the Left Ventricle, Liver, and One Venous Blood Sample. *Mol. Imaging* **2010**, *9*, 76−86.
(65) Hamblett, K. J.; Senter, P. D.; Chace, D. F.; Sun, M. M. C.; Lenox, J.; Cervent, C. G.; Kissler, K. M.; Bernhardt, S. X.; Kopcha, A. K.; Zabinski, R. F.; Meyer, D. L.; Francisco, J. A. Effects of Drug Loading on the Antitumor Activity of a Monoclonal Antibody Drug Conjugate. *Clin. Cancer Res.* **2004**, *10*, 7063−7070.
(66) Li, W. P.; Meyer, L. A.; Capretto, D. A.; Sherman, C. D.; Anderson, C. J. Receptor-Binding, Biodistribution, and Metabolism Studies of ^{64}Cu-DOTA-Cetuximab, a PET Imaging Agent for Epidermal Growth-Factor Receptor-Positive Tumors. *Cancer Biother. Radiopharm.* **2008**, *23*, 158−171.
(67) Yu, M.; Zheng, J. Clearance Pathways and Tumor Targeting of Imaging Nanoparticles. *ACS Nano* **2015**, *9*, 6655−6674.
(68) Barua, S.; Yoo, J. W.; Kolhar, P.; Wakankar, A.; Gokarn, Y. R.; Mitragotri, S. Particle Shape Enhances Specificity of Antibody-Displaying Nanoparticles. *Proc. Natl. Acad. Sci. U. S. A.* **2013**, *110*, 3270−3275.
(69) Melancon, M. P.; Lu, W.; Yang, Z.; Zhang, R.; Cheng, Z.; Elliot, A. M.; Stafford, R. J.; Olson, T.; Zhang, J. Z.; Li, C. *In Vitro* and *In Vivo* Targeting of Hollow Gold Nanoshells Directed at Epidermal Growth Factor Receptor for Photothermal Ablation Therapy. *Mol. Cancer Ther.* **2008**, *7*, 1730−1739.
(70) Wilhelm, S.; Tavares, A. J.; Dai, Q.; Ohta, S.; Audet, J.; Dvorak, H. F.; Chan, W. C. W. Analysis of Nanoparticle Delivery to Tumours. *Nat. Rev. Mater.* **2016**, *1*, 1−12.
(71) Kirpotin, D. B.; Drummond, D. C.; Shao, Y.; Shalaby, M. R.; Hong, K.; Nielsen, U. B.; Marks, J. D.; Benz, C. C.; Park, J. W. Antibody Targeting of Long-Circulating Lipidic Nanoparticles Does Not Increase Tumor Localization but Does Increase Internalization in Animal Models. *Cancer Res.* **2006**, *66*, 6732−6740.
(72) Mamot, C.; Drummond, D. C.; Noble, C. O.; Kallab, V.; Guo, Z.; Hong, K.; Kirpotin, D. B.; Park, J. W. Epidermal Growth Factor Receptor−Targeted Immunoliposomes Significantly Enhance the Efficacy of Multiple Anticancer Drugs *In Vivo*. *Cancer Res.* **2005**, *65*, 11631−11638.

DOI: 10.1021/acs.molpharmaceut.6b00566
Mol. Pharmaceutics 2016, 13, 3764−3772